Controlling factors of T_c dome structure in 1111-type iron arsenide superconductors

Satoru Matsuishi,[1,*] Takuya Maruyama,[2] Soshi Iimura,[2] and Hideo Hosono[1,2,3]

[1]*Materials Research Center for Element Strategy, Tokyo Institute of Technology, 4259 Nagatsuta-cho, Midori-ku, Yokohama 226-8503, Japan*

[2]*Materials and Structures Laboratory, Tokyo Institute of Technology, 4259 Nagatsuta-cho, Midori-ku, Yokohama 226-8503, Japan*

[3]*Frontier Research Center, Tokyo Institute of Technology, 4259 Nagatsuta-cho, Midori-ku, Yokohama 226-8503, Japan*

(Received 16 December 2013; revised manuscript received 10 February 2014; published 11 March 2014)

We investigated the effects of phosphorus substitution on the shape of the $T_c(x)$ dome in 1111-type $SmFeAs_{1-y}P_yO_{1-x}H_x$ ($0 < x < 0.5$). Hydride ion substitution of oxide sites ($O^{2-} \rightarrow H^-$) exerts a chemical pressure effect, i.e., a structural reduction of the *Pn*-Fe-*Pn* angle α (*Pn* = P, As) and also dopes electrons into the Fe*Pn* layer to induce superconductivity. Isovalent phosphorus substitution ($P^{3-} \rightarrow As^{3-}$) can induce only a chemical pressure effect, i.e., an increase of α for La substitution of Sm sites. As y increases from 0.0 to 0.5, the single T_c dome gradually splits into two domes, similar to those of $LaFeAsO_{1-x}H_x$ with a T_c valley at $x \approx 0.16$. We found that the T_c valley is located around $(x, \alpha) \approx (0.16, 113°)$ for both of the $SmFeAs_{1-y}P_yO_{1-x}H_x$ and $LaFeAsO_{1-x}H_x$ series, irrespective of changes in the *Pn* anion and *Ln* cation species. This result suggests that suppression of T_c leads to the emergence of a T_c valley when both the shape of FePn_4 tetrahedra represented by α and electron-doping level of x meet the above criterion in 1111-type iron oxypnictide superconductors.

DOI: 10.1103/PhysRevB.89.094510 PACS number(s): 74.70.Xa, 74.62.Bf, 74.25.F−

I. INTRODUCTION

1111-type *Ln*FeAsO (*Ln* = lanthanide) composed of an FeAs conducting layer and a *Ln*O insulating layer is a prototypical parent compound of iron-based superconductors [1–8] showing a tetragonal-orthorhombic structural transition at 120–160 K accompanied by antiferromagnetic (AFM) ordering of Fe spins [9–11]. Superconductivity, with a critical temperature T_c of up to 57.8 K [12,13], emerges when the structural-magnetic transition is suppressed by electron doping of the FeAs layer via fluoride-ion (F^-) substitution of oxygen sites. The doped electron concentration x vs temperature T diagram of $LnFeAsO_{1-x}F_x$ possess a superconducting (SC) region in the range $x = 0.1$–0.2 adjacent to an AFM region at $x \approx 0.0$ [14], although the whole shape of the SC region has not been determined because the solubility limit of F^- restricts x to <0.2. The SC region adjacent to the AFM region is a common feature of the electronic phase diagram for many unconventional superconductors, including iron pnictides [15]. Therefore, the electronic structure of $LnFeAsO_{1-x}F_x$ has been well studied, and the material dependence of T_c on the spin-fluctuation-mediated pairing mechanism has been explained to some degree [16–19].

Recently, we found that the SC region continues beyond $x \approx 0.4$ far from the AFM region by inducing high electron doping, with x up to 0.5, using hydride-ion (H^-) substitution in place of F^- [20–23]. In particular, $LaFeAsO_{1-x}H_x$ features a SC region with a unique shape that consists of a conventional dome (SC1) around $x \approx 0.1$ with a maximum T_c (T_c^{max}) of 29 K and an additional dome (SC2) around $x \approx 0.3$ with a T_c^{max} of 36 K. Inelastic neutron-scattering measurements of $LaFeAsO_{1-x}H_x$ revealed a switch of momentum transfer of magnetic excitation from 1.14 $Å^{-1}$ for the first dome to 1.25–1.38 $Å^{-1}$ for the second dome, indicating that the pairing channels for SC1 and SC2 regions are different from each other [24]. The split of the SC region, i.e., the emergence of double dome T_c structures, is an unexpected phenomenon in iron-based superconductors from theoretical studies. Thus, we consider that the elucidation of its origin is key to understanding the SC mechanism and to exploring the pathway to improve T_c.

Here we focus on the effects of physical and chemical pressure on the T_c-dome shape reported in Ref. [22]. When a physical pressure of up to 3 GPa was applied, the two SC regions for $LaFeAsO_{1-x}H_x$ merged into a single dome with $T_c^{max} = 47$ K. A similar phenomenon was also induced by replacement of La with Ce, Sm, and Gd. These results strongly suggest that the T_c-dome shape is controlled by the local structure of the $FeAs_4$ tetrahedron. As for the *Pn*-Fe-*Pn* angle α of the FePn_4 tetrahedron (*Pn* = P, As), Lee *et al.* have suggested that T_c increases as α approaches that of a regular tetrahedron [25]. Further, Kuroki *et al.* proposed on the basis of theoretical calculations that T_c is raised as the *Pn* height between the Fe plane h_{Pn} [18,19] is increased. However, because both structural parameters are related to each other by the equation $h_{Pn} = r_{Fe\text{-}Pn}\cos(\frac{\alpha}{2})$, where $r_{Fe\text{-}Pn}$ is the Fe-*Pn* bond length, it is difficult to distinguish which parameters of α and h_{Pn} have a dominant effect on the T_c-dome shape.

In this paper, we report the effects of phosphorus substitution on the $T_c(x)$-dome shape of 1111-type $SmFeAs_{1-y}P_yO_{1-x}H_x$ ($0 \le x < 0.5$). Isovalent P substitution of the As site ($P^{3-} \rightarrow As^{3-}$) induces a chemical pressure effect that changes α and h_{Pn} in a similar manner to that induced by La-substitution of the Sm site. As a result, we found double dome-shaped SC regions in $y = 0.45$ and 0.53. Because P substitution changes $r_{Fe\text{-}Pn}$, the resulting crystal structure can access the region in (α, h_{Pn}) space unexplored by *Ln* substitution. By considering the behavior of α and h_{Pn} in $SmFeAs_{1-y}P_yO_{1-x}H_x$ and $LnFeAsO_{1-x}H_x$ (*Ln* = La, Ce, Sm) systems, we discuss the controlling factors for the $T_c(x)$-dome shape of 1111-type Fe pnictides.

II. EXPERIMENTAL

$SmFeAs_{1-y}P_yO_{1-x}H_x$ with nominal y (y_{nom}) = 0.3, 0.5, and 0.6 were synthesized by the solid-state reaction of SmAs, FeAs, Fe_2As, Fe_2P, Sm_2O_3, and SmH_2 using a belt-type high

*Corresponding author: matsuishi.s.aa@m.titech.ac.jp

pressure anvil cell. The metal arsenides and phosphides were prepared from their respective metals. SmH_2 was synthesized by heating metal samarium in a H_2 atmosphere. All starting materials and precursors for the synthesis were prepared in a glove box filled with purified Ar gas (H_2O, $O_2 < 1$ ppm). The mixture of stating materials was placed into a BN capsule with a mixture of $Ca(OH)_2$ and $NaBH_4$ as an excess hydrogen source and then heated at 1473 K and 2 GPa for 30 min.

The amount of hydrogen incorporated into the resulting samples was evaluated by thermal desorption spectroscopy (TDS; ESCO TDS1200). Approximately 5 mg of the sample was heated to 1373 K at a heating rate of 60 K/min under vacuum $<10^{-6}$ Pa. Hydrogen released from the sample, in the form of H_2 molecules, was ionized and detected by a quadrupole mass spectrometer as an ion with mass-to-charge ratio $(m/z) = 2$. Other nonhydrogen elemental compositions (Sm: Fe: As: P: O) were determined by an electron-probe microanalyzer (EPMA; JEOL model JXA-8530F) equipped with a field-emission-type electron gun and wavelength dispersive x-ray detector. The micrometer-scale compositions within the main phase were probed on five to 10 focal points, and the results were averaged.

Phase purity of the resulting samples was determined by powder x-ray diffraction (XRD) using a Bruker diffractometer model D8 ADVANCE (Cu rotating anode). The crystallographic parameters of the synthesized 1111-type compounds were determined by Rietveld analysis of XRD patterns using TOPAS code [26], assuming a tetragonal symmetry (space group of $P4/nmmz$, lattice parameters $a = b \approx 0.39$ nm and $c \approx 0.84$ nm) with atomic positions of Sm (1/4, 1/4, z_{Sm}), Fe (3/4, 1/4, 1/2), Pn (1/4, 1/4, z_{Pn}), and O (3/4, 1/4, 0). During the refinement of structural parameters, site occupancies of Pn and O sites were fixed to the values estimated by the EPMA.

Four-probe dc resistivity (ρ) and magnetic susceptibility (χ) were measured in the temperature range 2–300 K, using a physical properties measurement system (Quantum Design, Inc.) with a vibrating sample magnetometer attachment.

III. RESULTS AND DISCUSSION

A. P-substitution effect on α and h_{Pn}

Using high pressure techniques, we obtained polycrystalline pellets containing >80 weight% of the 1111-type phase of $SmFeAs_{1-y}P_yO_{1-x}H_x$ ($0 \le x < 0.5$). The elemental composition analysis indicates that actual phosphorous content y tended to be less than the nominal content y_{nom} of the starting mixtures. As a result, we obtained samples with y values of ≈0.23, ≈0.45, and ≈0.53 from starting mixtures with $y_{nom} =$ 0.3, 0.5, and 0.6, respectively. The composition analysis is described in detail in the Supplemental Material [27]. The amount of oxide vacancies measured almost matched the hydrogen content, indicating that the oxide ions are successfully replaced by hydride to form $SmFeAs_{1-y}P_yO_{1-x}H_x$. Previous neutron diffraction analysis and density functional theory calculations demonstrated that the hydrogen exclusively replaces O^{2-} sites in the form of H^- ions and supplies an electron to the FePn layer to maintain charge neutrality [21].

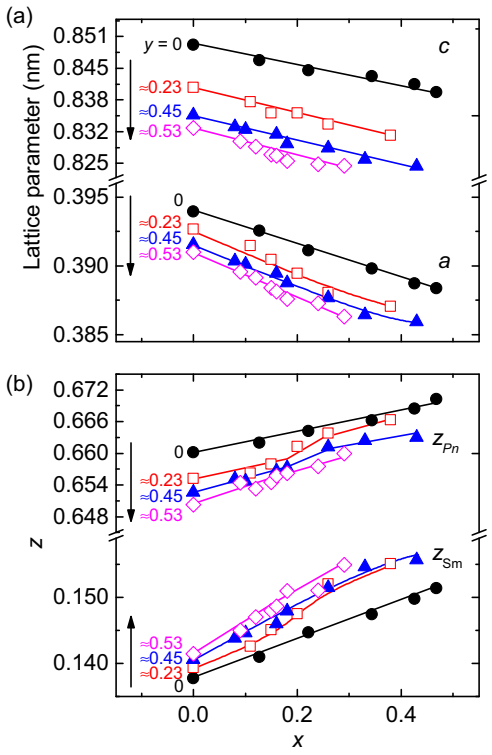

FIG. 1. (Color online) Crystallographic parameters of $SmFeAs_{1-y}P_yO_{1-x}H_x$ with $y = 0$, ≈0.23, ≈0.45, and ≈0.53 as a function of x. (a) Lattice parameters a and c. (b) z coordinate of Sm and Pn sites (z_{Sm} and z_{Pn}). Parameters for $y = 0$ are taken from previous literature [20].

Figures 1(a) and 1(b) show the variations in the lattice parameters (a and c) and z coordinate of Sm and Pn sites (z_{Sm} and z_{Pn}) as a function of x in $SmFeAs_{1-y}P_yO_{1-x}H_x$ specified by $y = 0$, ≈0.23, ≈0.45, and ≈0.53. With increases in x, the lattice parameters decrease, and the z coordinates increase, i.e., Sm_4O and FePn_4 tetrahedra become stretched along the c axis upon compression of the crystal lattice. With increases in y, $a(x)$ and $c(x)$ curves are shifted down, and the $z_{Sm}(x)$ curve is shifted up, indicating that the effects of P substitution on these parameters are the same as those of H substitution. In contrast, the effect of P substitution on z_{Pn} is the opposite to that of H substitution. Because P-substitution effects are the same as those of La and Ce substitution of Sm sites, the ranges of the geometric parameters of FePn_4 tetrahedron, i.e., α and h_{Pn} in $SmFeAs_{1-y}P_yO_{1-x}H_x$, partially overlap with those of the LnFeAs$O_{1-x}H_x$ (Ln = La–Sm) system.

Figure 2 shows α vs h_{Pn} plots for LnFeAs$O_{1-x}H_x$ and $SmFeAs_{1-y}P_yO_{1-x}H_x$. All the points of LnFeAsO_{1-x}H are located within a narrow bandlike region corresponding to $r_{Fe\text{-}Pn} = 0.239$–0.243 nm. In contrast to Ln or H substitution, which increases $r_{Fe\text{-}Pn}$ (+2 pm for 50% H substitution and full substitution of La to Sm), P substitution decreases $r_{Fe\text{-}Pn}$ (−7 pm for 50% P substitution) and expands the observable range in (α, h_{Pn}) space to allow investigation of the structural dependence of the T_c-dome shape.

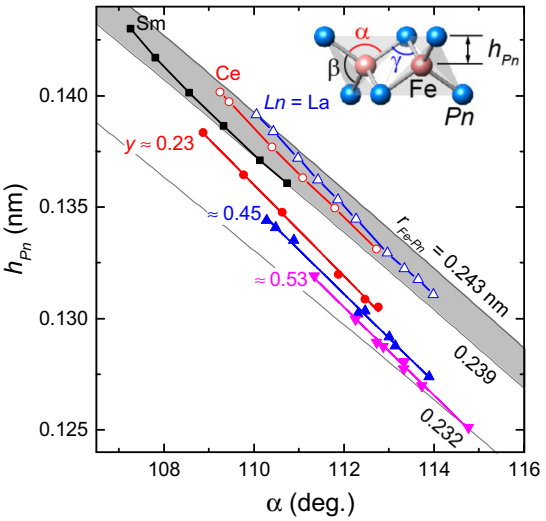

FIG. 2. (Color online) α vs h_{Pn} plots of LnFeAsO$_{1-x}$H$_x$ (Ln = La, Ce, and Sm) [22] and SmFeAs$_{1-y}$P$_y$O$_{1-x}$H$_x$ (y = 0.23, 0.45, and 0.53). Inset is a drawing of edge-shared FePn_4 tetrahedra in LnFePnO with notation of α (Pn-Fe-Pn), β (another Pn-Fe-Pn), and γ (Fe-Pn-Fe) angles and pnictogen height h_{Pn}. Lines are guides to the eye, tracing the α-h_{Pn} relation for specified y and Ln. In LnFeAsO$_{1-x}$H$_x$, the change in Fe-As bond length is small ($r_{Fe\text{-}Pn}$ = 0.239–0.243 nm), and h_{Pn} is strongly linked to α. By replacing As by P, $r_{Fe\text{-}Pn}$ clearly decreases.

B. P-substitution effect on T_c-dome shape

Figure 3(a) shows the temperature dependence of resistivity for $y \approx 0.23$. At $x = 0$, a kink in resistivity due to structural-magnetic transitions was observed around 90 K. As x increases, a sudden drop in resistivity to zero was observed at $x > 0.11$. The maximum onset T_c was 44.5 K at $x = 0.20$, and this decreased to <2 K at $x = 0.38$. For $y \approx 0.45$, as shown in Fig. 3(b), superconductivity was also observed at $x > 0.08$. The T_c decreased from 22.5 K at $x = 0.08$ to 18 K at $x = 0.16$ but subsequently increased to 24 K at $x = 0.21$. Finally, T_c decreased to <2 K at $x = 0.43$. A similar drop in T_c at $x = 0.16$ was also observed for $y \approx 0.53$ [see Fig. 3(c)]. $T_c = 4$ K was observed at $x = 0.15$ between $x = 0.12$ and 0.18, showing $T_c^{max} = 14$ K [27]. It is notable that a drop of resistivity was observed at ≈5 K in the x = 0.0 sample with $y \approx 0.53$. Because a drop in magnetic susceptibility was not observed in this temperature region, it is likely to originate from an AFM transition of Sm^{3+} spins similar to that observed in SmFePO [28]. Behavior observed in χ-T profiles also reflected the development of bulk superconductivity, as shown in Figs. 3(d)–3(f). A drop in susceptibility due to SC transitions was observed at the magnetic onset T_c^{mag}, which was slightly lower than the resistivity onset T_c. As shown in Figs. 3(e) and 3(f), a drop of T_c^{mag} was observed at x = 0.15–0.16 for $y \approx 0.45$ and 0.53. Figure 4 summarizes the magnetic onset T_c^{mag} as a function of x. A T_c^{mag} (x) curve for $y = 0$ taken from a previous paper [22] is also shown in this

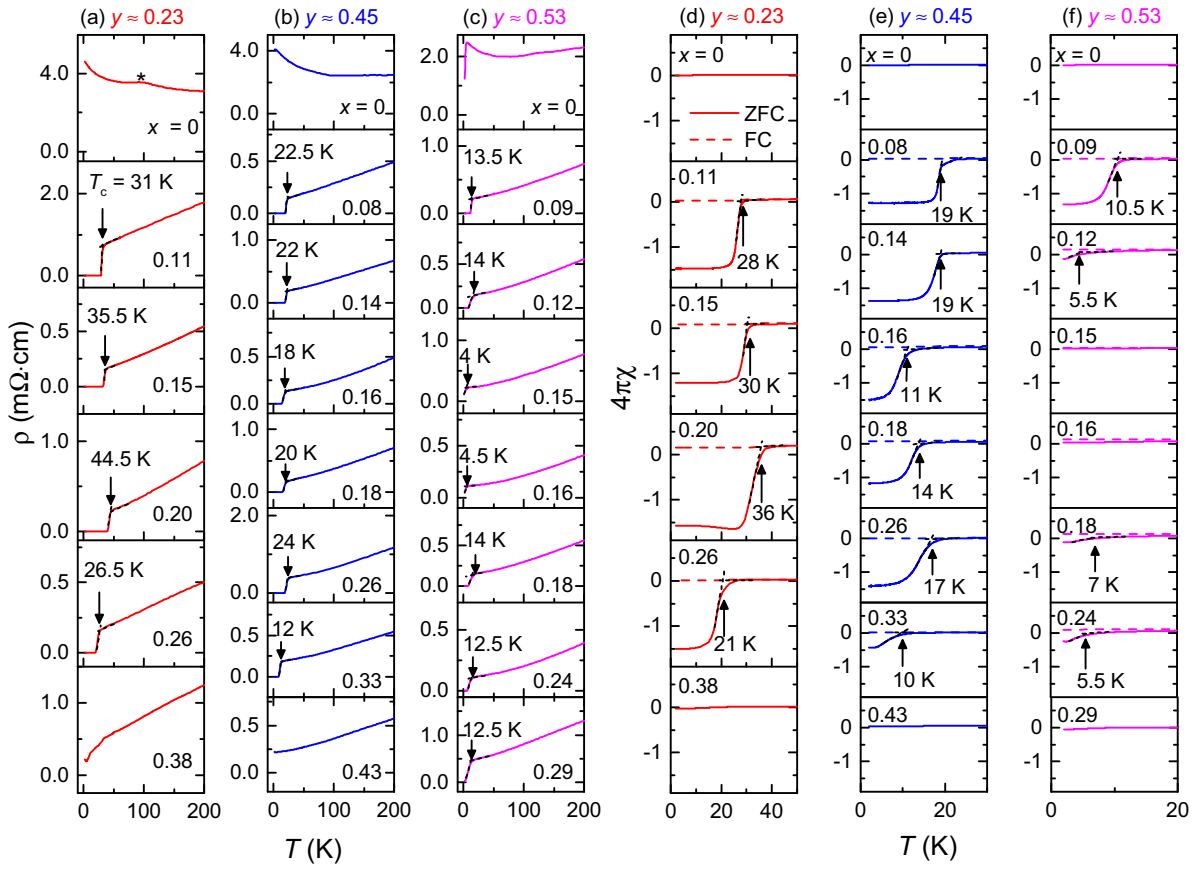

FIG. 3. (Color online) Temperature dependence of electrical resistivity (a)–(c) and magnetic susceptibility (b)–(f) in SmFeAs$_{1-y}$P$_y$O$_{1-x}$H$_x$ with $y \approx 0.23$, ≈0.45, and ≈0.53.

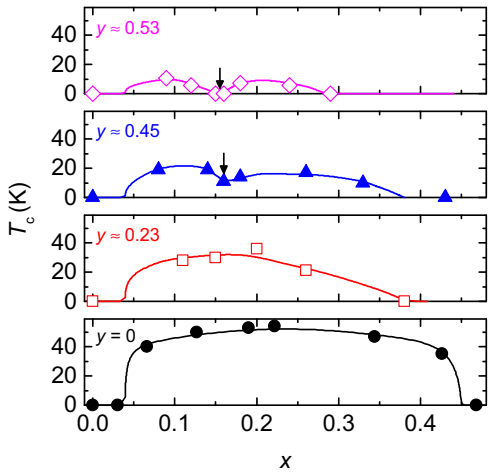

FIG. 4. (Color online) Magnetic onset T_c of $SmFeAs_{1-y}P_yO_{1-x}H_x$ as a function of x with $y = 0$, ≈0.23, ≈0.45, and ≈0.53. T_c values of $y = 0$ samples were taken from Ref. [20].

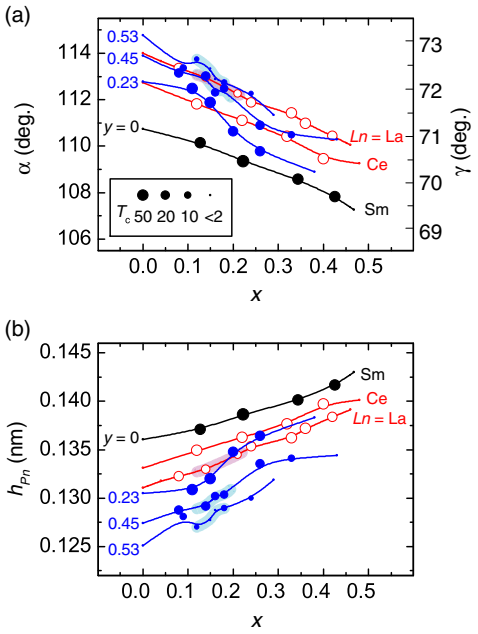

FIG. 5. (Color online) Correlation between the emergence of the T_c valley and structural or doping parameters in $SmFeAs_{1-y}P_yO_{1-x}H_x$ ($y = 0$, ≈0.23, ≈0.45, and ≈ 0.53; blue solid symbols) and $LnFeAsO_{1-x}H_x$ (Ln = La and Ce; red empty symbols). (a) α angle of FePn_4 tetrahedron as a function of x. Lines are guides to the eye, tracing $\alpha(x)$ for specified y and Ln. The symbol size indicates the T_c value. The region of the T_c valley for $SmFeAs_{1-y}P_yO_{1-x}H_x$ is denoted by a light blue area around $(x, \alpha) = (0.16, 113)$, which overlaps with that of $LaFeAsO_{1-x}H_x$ (denoted by a light pink colored area). (b) h_{Pn} vs x plot. The regions of the T_c valleys in each system do not overlap.

figure. In contrast to the single dome-shaped SC region for $y = 0$ and ≈0.23, a small valley is found at the center of the SC region in the $y \approx 0.45$ system. The split of the SC region was enhanced by further increase in y and the non-SC region ($T_c < 2$ K) was found at $x \approx 0.16$ in the $y \approx 0.53$ series.

C. T_c valley on x-α and x-h_{Pn} spaces

Figure 5(a) is an α vs x plot for $SmFeAs_{1-y}P_yO_{1-x}H_x$ and $LnFeAsO_{1-x}H_x$. The symbol size of each point represents the T_c value. Because of the chemical pressure effect of H substitution, the $\alpha(x)$ curve of $SmFeAsO_{1-x}H_x$ has a negative slope, and its intercept α_0 at $x = 0$ increases with P or La/Ce substitution of Sm sites. Therefore, the ranges of $\alpha(x)$ curves for $y = 0.23$–0.53 overlap with those for Ln = La, Ce. The regions of the T_c valleys for $y = 0.45$ and 0.53 are denoted by a light blue area and those for Ln = La by a light pink area. Both regions are clearly located at the same area around (x, α) = (≈0.16, ≈113°). In other words, double dome-shaped $T_c(x)$ curves are observed when the $\alpha(x)$ curve has a relatively large α_0 (>114°) and passes through the region around (≈0.16, ≈113°). Figure 5(b) is an analogous x vs h_{Pn} plot. In x-h_{Pn} space, the T_c valley for $y = 0.45$–0.53 is located at a position with different h_{Pn} (0.130 nm for $y = 0.45$–0.53; 0.134 nm for Ln = La). In addition, a drop of T_c is not observed in the $y \approx 0.23$ series, while their $h_{Pn}(x)$ curve crosses the region of the T_c valley of $LaFeAsO_{1-x}H_x$. These results indicate that the emergence of a T_c valley depends on α and not h_{Pn}, irrespective of the Pn anion and Ln cation species.

Finally, we discuss the effects of α on T_c. Parallel to this study, we have discovered the AFM ordering of iron spins with Néel temperature T_N up to 89 K in electron over-doped $LaFeAsO_{1-x}H_x$ ($x = 0.45$ and 0.51) [29]. The magnetic phase has a unique noncentrosymmetric structure different from that of the conventional AFM phase located at $x \sim 0.0$. This result suggests that the first and the second T_c domes in $LaFeAsO_{1-x}H_x$ come from different parent phases. Based on this idea, the result of the present study indicates that the T_c valley is a position where two SC phases encounter with each other, and their relationship becomes noncompetitive with the decrease of α. Because of the relationship between α and T_c in $LnFePnO_{1-x}H_x$, the "pairing glue" that induces superconductivity appears to depend on α. A candidate for this glue is the electron-phonon interaction associated with α. Saito *et al.* suggested in their orbital fluctuation theory that electron-phonon interactions are strongest when the $FeAs_4$ tetrahedron has a regular shape ($\alpha = 109.5°$) [30]. This theory can empirically explain the maximum T_c occurring when α is 109.5°. However, in comparing the α and x dependence of T_c, the resulting T_c-α relation is not monotonic but does depend on x. Another possibility is spin fluctuation enhanced by hopping between Fe $3d$ orbitals via As $4p$ orbitals. The hopping integral, i.e., the overlap integral of Fe $3d$ and As $4p$ orbitals, is directly determined by the Fe-As-Fe angle γ having a one-to-one relation with α: $\sin(\gamma/2) = 1/\sqrt{2} \cdot \sin(\alpha/2)$. In Fig. 5(a), the right vertical axis represents the γ value corresponding to α, and we can confirm that the T_c valley is located at $\gamma \sim 72°$.

Very recently, a calculation using the fluctuation exchange approximation successfully reproduced the shape variation of T_c-x with α in a $LnFeAsO_{1-x}H_x$ system from a double dome shape at large α to a single dome shape at small α [31]. The primary suggestion by this calculation is that the spin-fluctuation enhancement mechanism is different between low x and high x regions. The spin fluctuation in the former

region is caused by nesting of a Fermi surface composed of Fe $3d_{xz,yz}$ and $3d_{xy}$ orbitals, while that of the latter originates from real space motion of electrons within the $3d_{xy}$ orbitals, i.e., next-nearest-neighbor diagonal hopping (t_2) dominates the nearest-neighbor hopping (t_1). In this scheme, α plays an important role in determining the magnitude of spin fluctuations and T_c because both t_2 and indirect t_1 (t_1^{indirect}) are controlled by hopping via As $4p$ orbitals. Given the experimental findings and the theoretical real-space picture of electronic spin, α is the decisive factor for the shape variation of T_c-x in $Ln\text{FeAsO}_{1-x}\text{H}_x$ systems.

IV. SUMMARY

We found a double dome-shaped SC region in the x-T diagram of $\text{SmFeAs}_{1-y}\text{P}_y\text{O}_{1-x}\text{H}_x$ with $y = 0.45$ and 0.53. This finding agrees with previous results on $\text{LaFeAsO}_{1-x}\text{H}_x$. By investigating the correlation between T_c and structural parameters of the FePn_4 tetrahedron, we confirmed that the T_c valley separating the two SC domes is located at $x \approx 0.16$ and $\alpha \approx 113°$ in both $\text{SmFeAs}_{1-y}\text{P}_y\text{O}_{1-x}\text{H}_x$ and $\text{LaFeAsO}_{1-x}\text{H}_x$ systems. These results indicate that the emergence of two SC domes is generally induced in 1111-type iron oxypnictides when the electron-doping level matches the shape of the FePn_4 tetrahedron.

ACKNOWLEDGMENT

This work was supported by the JSPS FIRST project and the MEXT Element Strategy Initiative project.

[1] Y. Kamihara, T. Watanabe, M. Hirano, and H. Hosono, J. Am. Chem. Soc. **130**, 3296 (2008).
[2] H. Takahashi, K. Igawa, K. Arii, Y. Kamihara, M. Hirano, and H. Hosono, Nature **453**, 376 (2008).
[3] G. F. Chen, Z. Li, D. Wu, G. Li, W. Z. Hu, J. Dong, P. Zheng, J. L. Luo, and N. L. Wang, Phys. Rev. Lett. **100**, 247002 (2008).
[4] Z. A. Ren, J. Yang, W. Lu, W. Yi, G. C. Che, X. L. Dong, L. L. Sun, and Z. X. Zhao, Mater. Res. Innovations **12**, 105 (2008).
[5] C. Gen-Fu, L. Zheng, W. Dan, D. Jing, L. Gang, H. Wan-Zheng, Z. Ping, L. Jian-Lin, and W. Nan-Lin, Chin. Phys. Lett. **25**, 2235 (2008).
[6] Z.-A. Ren, J. Yang, W. Lu, W. Yi, X.-L. Shen, Z.-C. Li, G.-C. Che, X.-L. Dong, L.-L. Sun, F. Zhou, and Z.-X. Zhao, Europhys. Lett. **82**, 57002 (2008).
[7] X. H. Chen, T. Wu, G. Wu, R. H. Liu, H. Chen, and D. F. Fang, Nature **453**, 761 (2008).
[8] Z.-A. Ren, W. Lu, J. Yang, W. Yi, X.-L. Shen, Z.-C. Li, G.-C. Che, X.-L. Dong, L.-L. Sun, F. Zhou and Z.-X. Zhao, Chin. Phys. Lett. **25**, 2215 (2008).
[9] C. de la Cruz, Q. Huang, J. W. Lynn, J. Li, W. Ratcliff, II, J. L. Zarestky, H. A. Mook, G. F. Chen, J. L. Luo, N. L. Wang, and P. Dai, Nature **453**, 899 (2008).
[10] T. Nomura, S. W. Kim, Y. Kamihara, M. Hirano, P. V. Sushko, K. Kato, M. Takata, A. L. Shluger, and H. Hosono, Supercond. Sci. Technol. **21**, 125028 (2008).
[11] J. Zhao, Q. Huang, C. de la Cruz, S. Li, J. W. Lynn, Y. Chen, M. A. Green, G. F. Chen, G. Li, Z. Li, J. L. Luo, N. L. Wang, and P. Dai, Nat Mater **7**, 953 (2008).
[12] C. Wang, Z. Gao, L. Wang, Y. Qi, D. Wang, C. Yao, Z. Zhang, and Y. Ma, Supercond. Sci. Technol. **23**, 055002 (2010).
[13] M. Fujioka, S. J. Denholme, T. Ozaki, H. Okazaki, K. Deguchi, S. Demura, H. Hara, T. Watanabe, H. Takeya, T. Yamaguchi, H. Kumakura, and Y. Takano, J. Phys. Soc. Jpn. **82**, 094707 (2013).
[14] C. Hess, A. Kondrat, A. Narduzzo, J. E. Hamann-Borrero, R. Klingeler, J. Werner, G. Behr, and B. Büchner, Europhys. Lett. **87**, 17005 (2009).
[15] C. W. Chu, Nat. Phys. **5**, 787 (2009).
[16] I. I. Mazin, D. J. Singh, M. D. Johannes, and M. H. Du, Phys. Rev. Lett. **101**, 057003 (2008).
[17] K. Kuroki, S. Onari, R. Arita, H. Usui, Y. Tanaka, H. Kontani, and H. Aoki, Phys. Rev. Lett. **101**, 087004 (2008).
[18] K. Kuroki, H. Usui, S. Onari, R. Arita, and H. Aoki, Phys. Rev. B **79**, 224511 (2009).
[19] K. Kuroki, J. Phys. Chem. Solids **72**, 307 (2011).
[20] T. Hanna, Y. Muraba, S. Matsuishi, N. Igawa, K. Kodama, S. I. Shamoto, and H. Hosono, Phys. Rev. B **84**, 024521 (2011).
[21] S. Matsuishi, T. Hanna, Y. Muraba, S. W. Kim, J. E. Kim, M. Takata, S. I. Shamoto, R. I. Smith, and H. Hosono, Phys. Rev. B **85**, 014514 (2012).
[22] S. Iimura, S. Matsuishi, H. Sato, T. Hanna, Y. Muraba, S. W. Kim, J. E. Kim, M. Takata, and H. Hosono, Nat. Commun. **3**, 943 (2012).
[23] H. Hosono and S. Matsuishi, Curr. Opin. Solid State Mater. Sci. **17**, 49 (2013).
[24] S. Iimura, S. Matsuishi, M. Miyakawa, T. Taniguchi, K. Suzuki, H. Usui, K. Kuroki, R. Kajimoto, M. Nakamura, Y. Inamura, K. Ikeuchi, S. Ji, and H. Hosono, Phys. Rev. B **88**, 060501 (2013).
[25] C.-H. Lee, A. Iyo, H. Eisaki, H. Kito, M. T. Fernandez-Diaz, T. Ito, K. Kihou, H. Matsuhata, M. Braden, and K. Yamada, J. Phys. Soc. Jpn. **77**, 083704 (2008).
[26] Bruker AXS (2009).
[27] See Supplemental Material at http://link.aps.org/supplemental/10.1103/PhysRevB.89.094510 for compositions of $\text{SmFeAs}_{1-y}\text{P}_y\text{O}_{1-x}\text{H}_x$ measured by EPMA and TDS.
[28] Y. Kamihara, H. Hiramatsu, M. Hirano, Y. Kobayashi, S. Kitao, S. Higashitaniguchi, Y. Yoda, M. Seto, and H. Hosono, Phys. Rev. B **78**, 184512 (2008).
[29] M. Hiraishi, S. Iimura, K. M. Kojima, J. Yamaura, H. Hiraka, K. Ikeda, P. Miao, Y. Ishikawa, S. Torii, M. Miyazaki, I. Yamauchi, A. Koda, K. Ishii, M. Yoshida, J. Mizuki, R. Kadono, R. Kumai, T. Kamiyama, T. Otomo, Y. Murakami, S. Matuishi, and H. Hosono, Nat. Phys., doi:10.1038/nphys2906.
[30] T. Saito, S. Onari, and H. Kontani, Phys. Rev. B **82**, 144510 (2010).
[31] K. Suzuki, H. Usui, S. Iimura, Y. Sato, S. Matsuishi, H. Hosono, and K. Kuroki, arXiv:1311.2413.